Spontaneously-induced Magnetic Anisotropy in Ultrathin Co/MoS_2 Heterojunction

Chun-I Lu, Tzu-Hung Chuang, and Der-Hsin Wei*

Scientific Research Division, National Synchrotron Radiation Research Center, Hsinchu, Taiwan

Chih-Heng Huang

International PhD Program for Science,

National Sun Yat-Sen University, Kaohsiung, Taiwan

Kui-Hon Ou Yang

Graduate Institute of Applied Physics, National Taiwan University, Taipei, Taiwan

Minn-Tsong Lin

Department of Physics, National Taiwan University, Taipei, Taiwan

Institute of Atomic and Molecular Sciences, Academia Sinica, Taipei 10617, Taiwan

Kai-Shin Li

National Nano Device Laboratories, National Applied Research Laboratories, Hsinchu, Taiwan

Feng Li (419981588@qq.com), Junjie Qi (junjieqi@ustb.edu.cn)

State Key Laboratory for Advanced Metals and Materials, School of Materials Science and Engineering, University of Science and Technology Beijing, Beijing100083, People's Republic of China

Kristan Bryan Simbulan, Yann-Wen Lan†

Department of Physics, National Taiwan Normal University, Taipei, Taiwan

Matteo Jugovac, Iulia Cojocariu, Vitaliy Feyer, Christian Tusche

Forschungszentrum Jülich, Peter Grünberg Institut (PGI-6), 52425, Jülich, Germany

Abstract

Magnetic anisotropy (MA) is the basis of the architecture of magnetic-based devices and is referred to as the material preference in aligning its magnetization along a specific direction. Here, we report the discovery of a strong MA in cobalt-molybdenum disulfide (Co/MoS_2) heterojunction. Element-specific magnetic images recorded from the X-ray photoemission electron microscope (PEEM) reveal that ultrathin Co films, with a thickness of 5 monolayers (ML) and above, deposited on single-layer MoS_2 flakes show micrometer-sized domains at room temperature. Subsequent image analysis reveals that the domains magnetizations are not randomly oriented but are rather aligned to directions that are in apparent correlation to the MoS_2 crystal structure. Micro-area X-ray photoelectron spectroscopy (μ-XPS) analysis on the Co/MoS_2 heterojunction suggests that there is charge donation from cobalt to sulfur. Comparing to the distinct magnetic behavior previously reported for non-reactive Fe/MoS_2 heterojunctions, we suggest that orbital hybridization at the interface is a needed ingredient to facilitate the appearance of MA in Co/MoS_2 heterojunctions. Our report provides micro-magnetic evidences and micro-spectroscopic insights that consolidate the knowledge needed to build functional heterostructures based on two-dimensional materials.

keywords: TMDC, spintronics, XMCD, PEEM

INTRODUCTION

After the discovery of graphene, monolayer MoS_2 – a layered van der Waals (vdW) semiconducting transition metal dichalcogenide (TMD)[1, 2, 3, 4] – has emerged as another 2D material prototype, which can either be obtained by exfoliation from bulk crystal or grown via chemical vapor deposition (CVD)[5, 6]. The indirect bandgap of bulk MoS_2 changes to a direct bandgap as its thickness decreases to single layer[5, 7, 8]. Its promising semiconductor properties led few-layer MoS_2 to different types of applications, such as field-effect transistors, light-emitting diodes, and solar cells[9, 10, 11, 12]. Additionally, due to the strong spin-orbit coupling and the absence of inversion symmetry in the monolayer regime, spin splitting arises at the boundaries of the surface Brillouin zone, specifically,

at the **K** and **-K** points, to conserve the time-reversal symmetry[13, 14, 15]. Such a unique band structure provides the possibility to encode information through the material valley pseudospin. These valley-based electronics is coined as valleytronics, name inspired after another famous field called spintronics[16, 17, 18, 19].

Monolayer MoS_2 can also be used as a spacer in spin-valve devices, by exploiting its semiconducting nature and its stable spin-polarization in the out-of-plane transition direction[20, 21]. A spin-valve effect was experimentally demonstrated on the NiFe/MoS_2/NiFe structure, showing a magnetoresistance (MR) of 0.73% at 20 K and 0.23% at 240 K[22]. MR is defined as the electrical resistance difference between the parallel and the anti-parallel orientations of the two ferromagnetic (FM) electrodes attached on the MoS_2 material. The confirmation of spin-valve effect in MoS_2-based heterostructure proves that TMDs are potential candidates for spintronic applications, but the large discrepancy between the MRs that are measured experimentally (less than 1%)[22] and predicted theoretically (as large as 300%)[23] suggests that key players have yet to be identified.

Direct investigation on the fundamental magnetic properties of FM-TMD heterojunctions is known to be informative but remains scattered to this day. One of these studies examined the morphology of Fe thin films grown on the MoS_2 surface and the corresponding hysteresis loop via scanning tunneling microscopy (STM) and Kerr microscopy, respectively[24, 25]. The study found not only a formation of nanoparticles but also a magnetic decoupling between the Fe/MoS_2 and the Fe/SiO_2 interfaces. The reported X-ray photoemission spectroscopy (XPS) studies showed that there is no charge transfer between Fe and MoS_2[24, 25]. For the Co/MoS_2 heterojunction here studied, on the other hand, a first-principles calculation done by Garandel *et al.* revealed the possible existence of a spin-transfer effect at the Co/MoS_2 interface deriving from the covalent bonding between the S and Co atoms. Based on their calculation, Garandel *et al.* predicted that the MoS_2 layer could become metallic and spin-polarized[26].

In this report, by depositing Co ultrathin films onto the CVD-grown monolayer MoS_2 flakes[6], we experimentally examine the magnetic domain configuration of Co/MoS_2 heterojunction. The identification of Co magnetic domains has been performed by detecting the X-ray magnetic dichroism (XMCD) effect using a photoemission electron microscope[27]. μ-XPS spectra measurements[28] reveal that a charge transfer, induced by the formation of the covalent bond between S and Co atoms, occurs at the Co/MoS_2 interface. The magnetic domains are spontaneously formed on the Co layer, and the directions of the domain walls are following the underlying MoS_2 lattice

structure. Findings above imply that a magnetic anisotropy does exist in Co/MoS_2 heterojunction and the interplay between Co and MoS_2 is likely responsible for the domain configuration observed.

RESULTS

Figure 1 shows the optical images of the MoS_2 islands on SiO_2 substrate after the CVD growth process. The surface is composed of flakes of different shapes, i.e. star-like or triangular. The consistent transparency among MoS_2 flakes suggests that their thicknesses are almost identical. The collective photoluminescence (PL) and Raman spectra, shown in Figure 1(b) and (c), respectively, indicate that most of the MoS_2 flakes are monolayer. This is revealed by a peak-distance of 21 cm^{-1} between the two dominant peaks: E^1_{2g} at 383.8 cm^{-1} and A_{1g} at 404.1 cm^{-1} in the Raman spectra, as well as by a sharp peak intensity located at 1.8 eV in the PL spectra[5, 29].

The schematic band structure of a typical FM 3*d* transition material is drawn in Figure 2(a), in which a net magnetic moment is originated from the asymmetrical nature of the 3*d* band. According to the selection rules, an incident light with right or left circular polarization (RCP or LCP) excites electrons that fulfill the transition conditions: $\Delta s = 0$ and $\Delta m = \pm 1$. However, the probabilities of each pair of corresponding transitions, from the 2*p* core-level up to the 3*d* band, are not equal for majority and minority spin channels since the empty states that are available for transition are asymmetric. A schematic diagram of the experimental setup is illustrated in Figure 2(b), which shows an incident circularly polarized beam hitting the sample – a Co ultrathin film on MoS_2 – at a grazing incident angle of 20°. The spatial distribution of photo-emitted electrons induced by both the RCP and LCP incident beam can be resolved through PEEM, allowing the observation of magnetic domains in the Co layer due to the XMCD effect[30, 31]. In this study, domain images were enhanced by taking advantage of the absorption asymmetry and, thus, the actual asymmetry image was further processed as $I_A = (I_{L3} - I_{L2})/(I_{L3} + I_{L2})$, where I_{L2} and I_{L3} represent the image which is derived at photon energies (PE) equal to the transition edges L_2 and L_3, respectively. Since this image-processing can eliminate geometrical inhomogeneity, the contrast in the I_A image is used to recognize magnetic domains of different magnetization directions[32, 33]. Figure 2(c) shows the resulting XMCD image of a 9 ML Co film deposited on monolayer MoS_2. In the image, two regions of different contrasts are labeled as region A and B. The micro-area X-ray absorption spectroscopy (μ-XAS) spectra acquired on A and B domains (displayed in Figure 2(d)) were extracted from the stack of images recorded at a step of

0.2 eV from hν = 750 eV to 810 eV, across Co $L_{2,3}$ edges. The asymmetry between these two spectra, as displayed in the XMCD curve in the bottom portion of Figure 2(d), confirms that the color contrast in Figure 2(c) has a magnetic origin. Note that the exact magnetization direction of the domains cannot be determined since it was not possible to rotate the sample *in situ* and/or to apply an external magnetic field in the PEEM experimental chamber. Therefore, the system is only sensitive to whether the magnetic domains are parallel (brighter) or antiparallel (darker) with respect to the incident light.

Figure 3(a)-(c) show the XMCD images of Co films of different thicknesses (5 ML, 7 ML, and 9 ML). After the acquisition of the XMCD image of the 5 ML Co film, succeeding sets of images were also acquired for each additional bilayers grown on top of the sample. After comparing these images, we conclude that the domain shape tends to be independent of the film thickness; however, the image contrast is enhanced with thicker Co layers. The XMCD image can be conceived as the inner product of the sample magnetization ($\vec{M}$) and the beam polarization ($\vec{\sigma}$), i.e. $I \propto \vec{M} \cdot \vec{\sigma}$ [33]. In our case, the incident angle and the polarization of the photon beam are fixed; thus, the image contrast reflects the local orientation of the sample magnetic domains. Since Co coverage is assumed to be uniform on MoS_2[34], the magnitude of magnetization is fixed across the whole surface. Therefore, the dominant factor that produces contrast in XMCD images is the angle between the direction of the beam and domain magnetization. The histograms in Figure 3 depict the grayscale distribution of XMCD image contrast, which can be correlated to the angular distribution of magnetic domains. Therefore, the intensity distribution in the histogram represents the frequency of a particularly oriented magnetic domain in the sample. In the hypothetical case of out-of-plane magnetic domains, only two contrast levels would be observed, corresponding to the up or down magnetization directions. Since our histogram is composed of a distribution of contrast levels, we can conclude that the magnetization of the Co domains has limited orientations that are either canted or lying in-plane.

The XMCD-PEEM imaging reveals that the Co domain boundaries tend to have preferential directions. In fact, Figure 4(a) shows that the magnetic domains of a 9 ML Co film on a single crystalline monolayer MoS_2 flake are large and well ordered. In order to unravel the role of the MoS_2 crystallinity in the magnetic ordering of the domains, we grew a 9 ML Co film on a polycrystalline monolayer MoS_2[34], noticing, from the XMCD-PEEM result in Figure 4(b), that the domain becomes tiny and less-ordered. CVD-grown triangular MoS_2 flakes are usually treated as a single crystalline

grain, and the edge is always either in an armchair or in a zig-zag configuration[36]. Interestingly, we reveal (Figure 4(c)) that the domain walls of the 9 ML Co film deposited on triangular MoS_2 flakes are parallel to either the zigzag (red) or the armchair (blue) direction of the MoS_2 lattice. The two flakes, A and B, and their corresponding simplified 2H-MoS_2 ball models illustrated in Figure 4(d) clearly show this trend. We want to emphasize that the characterization has been performed also on other MoS_2 flakes, reaveling the same tendency observed in Figure 4(c). Such an observation suggests that the MoS_2 lattice structure plays an important role in manifesting the orientations of ferromagnetic Co domain[34].

XPS is a sensitive tool for analyzing the chemical environment of a specific element. Figure 5 shows the μ-XPS spectra acquired on the 4 ML Co/SiO_2 and the 4 ML Co/MoS_2 regions, respectively. Since the Co layer has been prepared *in-situ*, under UHV conditions, the Co 2p core levels acquired on the two different areas mainly contain contributions from Co(0) ($2p_{3/2}$ = 778.3 eV)[37], which corresponds to the unoxidized (metallic) state of Co. Moreover, apart from the signal corresponding to the Auger emission from the S atoms of the substrate, which suggests that the photoemission process is sensitive to the Co/MoS_2 interface, the two spectra have a non-negligible difference. The fit of the Co 2p core level acquired on Co/MoS_2 suggest the presence of additional peaks, namely Co(II) ($2p_{3/2}$ = 781.5 eV) and Co(III) ($2p_{3/2}$ = 779.7 eV) in comparison to Co/SiO_2[37, 38]. The origin of the weak Co(III) signal observed in the Co/SiO_2 region is suggested to be the Co oxidization induced by the interaction with the oxide substrate[39]. This phenomenon means that the charge transfer process is greater in the Co/MoS_2 heterojunction with respect to the Co/SiO_2 case. The charge transfer process involves electron donation from Co atoms to the MoS_2 substrate. It has to be noted that no intermixing occurs at the Co/MoS_2 interface since this would lead to the breaking of the bonds between the Mo and S atoms, and therefore a shift would have been observed in XPS[40]. Indeed, Mo 3d and S 2p μ-XPS spectra (Supplementary Figure S6) show that the bonding between the Mo and S atoms in the Co/MoS_2 heterojunction does not differ from that of the pristine MoS_2[29].

DISCUSSION

Based on the above observations, we confirm that the deposition of Co ultrathin film on MoS_2 flakes leads to the formation of spontaneous micro-meter sized ferromagnetic domains. The domain

boundaries have preferential directions, which are either parallel to the zig-zag or to the armchair directions of the MoS_2 structure. These findings imply that both the magnetic long-range ordering and magnetic anisotropy are present in this system. No external field is applied during the Co growth process and XMCD-PEEM measurements, which invalidates the possibility of domains forming induced by this external factor.

The crystalline anisotropy of the Co layer was initially considered to be a possible reason for the spontaneous creation of magnetic domains in Co/MoS_2. The magneto-behavior of ultrathin metallic films is tunable by adjusting the strains in the material lattice or even by changing its crystalline structure, i.e., by epitaxially depositing it on a suitable substrate. An example is BCC-Co, obtained by depositing it on a GaAs(110) substrate, which has a different Curie temperature and anisotropy compared to bulk HCP-Co[41]. However, as the low energy electron diffraction (LEED) results on Co/MoS_2 (bulk crystal) failed to produce a sharp pattern, we suspect that the growth of Co/MoS_2 (monolayer) might not be epitaxial; in fact, the Co layer grown on the MoS_2 surface seems amorphous[34]. We therefore suggest that the crystalline structure of Co can not be the only reason for the MA observed in Co/MoS_2 (monolayer). The observed magnetic behavior is not ascribed to shape anisotropy effects since the thickness of the Co layer is not comparable to the area of the MoS_2 flake (several nm *vs.* tens of μm^2).

Moreover, results of XPS suggest that a charge transfer from Co to MoS_2 exists. This finding is consistent with the theoretical work of Garandel *et al.* reporting that Co atoms at the interface tend to covalently bond to the topmost S atoms of the substrate, which is followed by the transferring of spin moments from Co to MoS_2. In addition, the calculated spin majority and minority in MoS_2 are suggested to have a space-dependent distribution in the MoS_2 lattice, induced by Co[26]. According to Garandel's work, a possible mechanism at the basis of the observed domains formation is described as follows. Firstly, due to the donated spin moment from the Co layer, the MoS_2 layer gets magnetized. The induced spatial spin asymmetry in MoS_2 can therefore form magnetic domains on the MoS_2 layer. These magnetic domains can couple back to the upper cobalt layer, effectively forming the Co domains, as observed in the experiment. The mechanism described above could explain why the domain boundaries are correlated to the lattice structure of MoS_2.

In conclusion, we prove that a CVD-grown monolayer MoS_2 flake facilitate the spontaneous formation of magnetic domains in the ultrathin Co film deposited on it. Furthermore, with the evidence of charge donation from Co to S in MoS_2, we argue that such interaction at the interface is what set apart the magnetic properties of Co/MoS_2 found here and Fe/MoS_2 reported earlier[24, 25]. We demonstrate that the ultrathin Co films form spontaneous magnetic domains upon deposition on a CVD-grown monolayer MoS_2. The shape of these domains indicates that monolayer MoS_2 induces magnetic anisotropy on cobalt, deriving from charge/spin transfer effect at the interface. It can also be noted that the charge transfer mechanism is the key factor in the implementation of the concept since, for other transition metals such as Fe, magnetic domains similar to Co were not observed. In fact, XPS studies from Hsu *et al.* show that there is no charge transfer between Fe and MoS_2[24, 25]. In view of spintronics, our work proves that the Co/MoS_2 interface can be a useful junction for future device applications.

METHODS

High-quality single-crystal monolayer MoS_2 flakes were grown inside a tubular furnace equipped with a 30 mm diameter quartz tube. The SiO_2/Si substrates were cleaned using a standard procedure and then soaked into a H_2SO_4/H_2O_2(3:1) solution for 2 h. 0.01 g of MoO_3 powder was then positioned on a silver quartz boat located at the heating zone of the furnace. The 2 cm × 2 cm-sized SiO_2/Si substrate was placed face down above the MoO_3 powder. The surfur powder was placed in a separate ceramic boat located at the upper stream of the furnace with a temperature of about 170 ℃. To carry both the S and the MoO_3-x vapors onto the target substrate, ultrahigh-purity Ar gas flow was used. Once all the above preparations were set, the temperature has to be kept at 120 ℃ (500 sccm) for 30 min, then ramped up to 850 ℃ at a rate of 20 ℃-min^{-1} (200 sccm), allowing the CVD growth of MoS_2. The sample is kept for 30 minutes more at the conditions above mentioned before allowing the sample to passively cool down to room temperature.

The MoS_2 samples grown on Si/SiO_2 substrates were loaded into the TLS05B2 endstation and heated at 150 ℃ for 6 h under ultra-high vacuum (UHV) in order to outgas them. The Co layers were grown using a commercial EFM3T, and their thickness is defined in units of monolayer (ML). The

Co deposition rate was determined by performing medium-energy electron diffraction (MEED) measurements while depositing them on a Cu(001). After Co deposition, the sample was transferred into the PEEM chamber[27] under UHV conditions for XMCD imaging. The XMCD images were leveled by subtracting the polynomial background, which is supposedly a consequence of the beam spot shifting brought about by a change in the photon energy.

The μ-XPS measurements were performed at the 1.2L NanoESCA beamline at Elettra Synchrotron in Trieste (Italy)[28]. Prior to cobalt deposition, the MoS_2/SiO_2 samples were outgassed at 250 ˚C in a UHV preparation chamber for 2 h. The acquisition of Co 2p spectra was performed using a 950 eV s-polarized photon energy. Thanks to the reduced beam spot size on the sample (<20 μm) it was possible to selectively collect μ-XPS spectra from Co/MoS_2 flakes and Co/SiO_2 regions.

DATA AVAILABILITY

All relevant data are available from the authors. Requests for data and materials should be addressed to D.-H. Wei.

ACKNOWLEDGMENTS

Thanks to the members of TLS09A1 and TLS09A2 for the suggestion of XPS data analysis and the prior test measurements. Especially thanks to Dr. Chia-Hao Chen, Dr. Yao-Jane Hsu, Dr. Hung-Wei Shiu, Dr. Li-Chung Yu, Dr. Shang-Hsien Hsieh and Dr. Lo-Yueh Chang. And thanks to Dr. Yao-Jui Chan in National Sun Yat-Sen University for the beamtime assistance. Also, thanks to Dr. Yu-Hsun Chu in National Taiwan University for the fruitful discussion. This work was supported in part by the Ministry of Science and Technology of Taiwan through grant No. MOST 104-2112-M-213-002-MY3 (D.-H. Wei), No. MOST 105-2112-M-213-012-MY2 (T.-H. Chuang) and No. MOST 105-2112-M-003-016-MY3 (Y.-W. Lan). This work was also in part supported by the National Nano Device Laboratories.

AUTHOR CONTRIBUTIONS

C.-I.L. performed PEEM with assistance from C.-H.H., and T.-H.C. The data analysis was performed by C.-I.L. and discussed in depth with C.H.H, T.-H.C., Y.-W.L. and D.-H.W. The monolayer MoS_2 flakes was grown by F.L., J. Q. and Y.-W.L. The polycrystalline monolayer MoS_2 was grown by K.-S.L. The μ-XPS were measured by C.-I.L. K.-H.OY., M.-T.L, C.-H.H. M.J., I.C., V.F., and C.T. The abroad study project in Elettra Synchrotron in Trieste (Italy) is proposed and conducted by T.-Z.C. The manuscript was prepared by C.-I.L. and D.-H.W. with assistance from K. B. S., V.F. and Y.-W.L. This project was conceived and led by D.-H.W.

COMPETING INTERESTS

The authors declare no competing interests.

*dhw@nsrrc.org.tw

†ywlan@ntnu.edu.tw

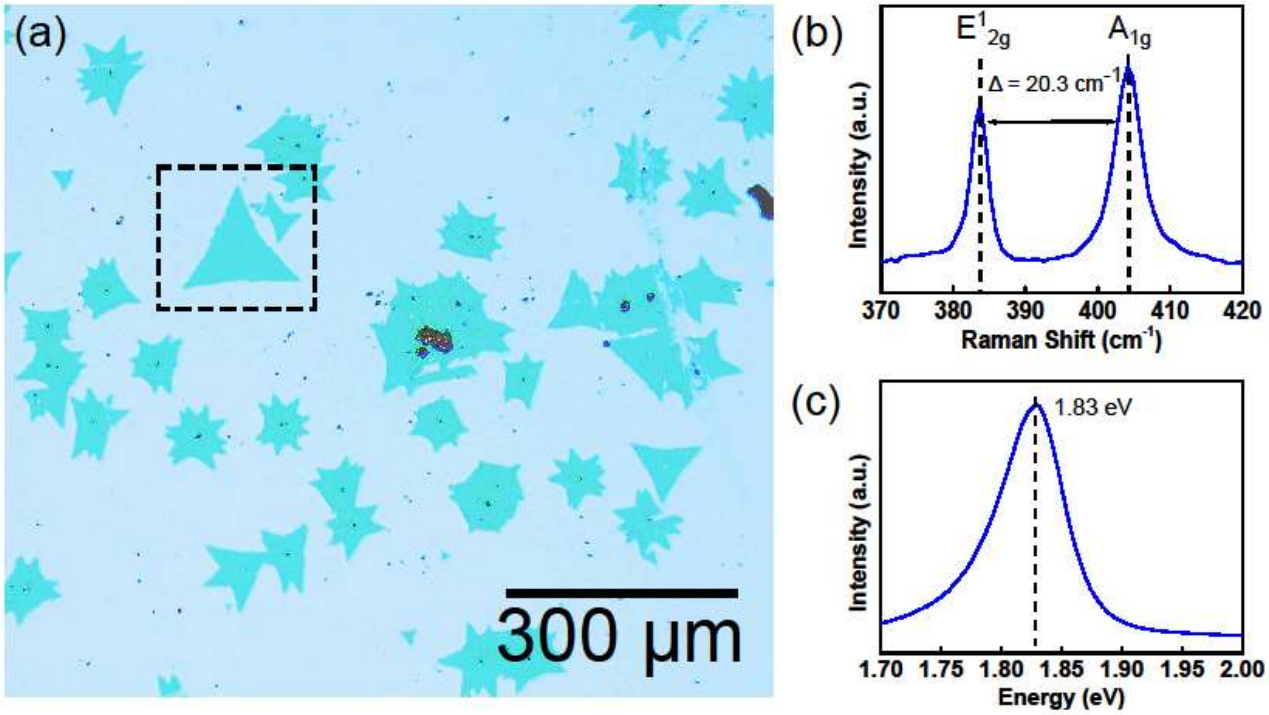

Figure 1: **Monolayer of MoS_2 (a)** OM image of the CVD-grown MoS_2 islands on SiO_2. The dashed square indicates a triangular MoS_2 sample, which is also featured in Figure 3. **(b)** The Raman spectrum of the sample shows two dominant Raman modes at 383 cm^{-1} and 404 cm^{-1} with a peak-distance of 21 cm^{-1}. **(c)** The PL spectrum of the sample indicates that the photoluminescence peak energy is equal to 1.83 eV. These two spectra indicate that the MoS_2 islands are monolayer.

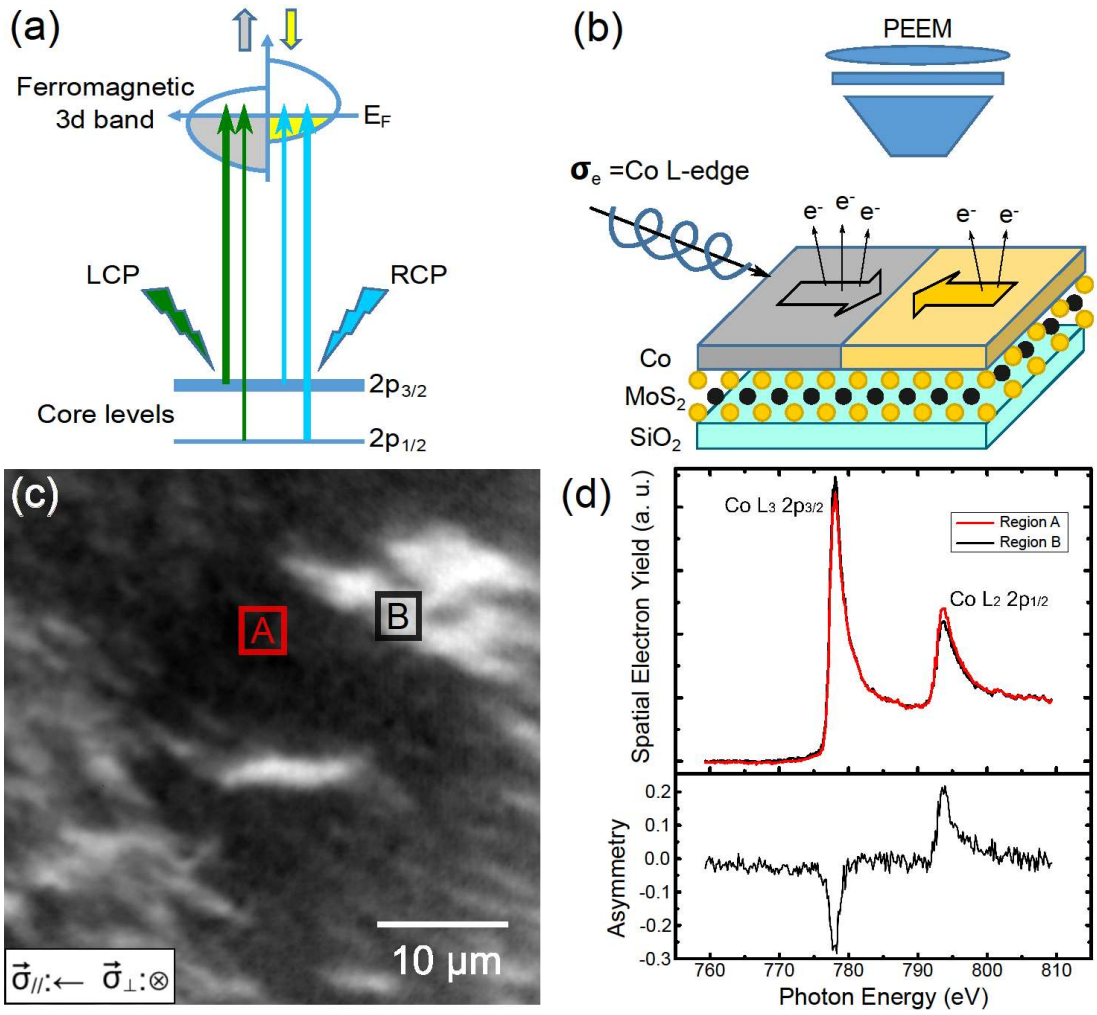

Figure 2: **XMCD (a)** A schematic diagram describing the principle of XMCD. The excitations of the spin-up and spin-down electrons from the 2p band are distinct when a circularly-polarized beam is applied along a particular magnetic domain. This asymmetry is reversed with the beam focused on the opposite magnetization domain. **(b)** A schematic diagram illustrating the experimental setup. The incident circularly polarized soft x-ray beam has a 20° angle with respect to the sample surface. Due to the effect of XMCD, opposite magnetic domains respond differently when the photon energy of the incident beam is resonant to the Co L_3 and L_2 edges. The emitted photoelectrons are collected by PEEM, which allows for spatial mapping of different magnetic domains. **(c)** XMCD image of 9 ML cobalt on monolayer MoS_2. The inset shows the incident light direction. **(d)** Corresponding μ-XAS spectra of regions A and B, whose positions are marked in (c), are shown. The bottom spectrum represents the asymmetrical nature of spectra A and B, which proves that the grayscale contrast in (c) is the consequence of the XMCD effect.

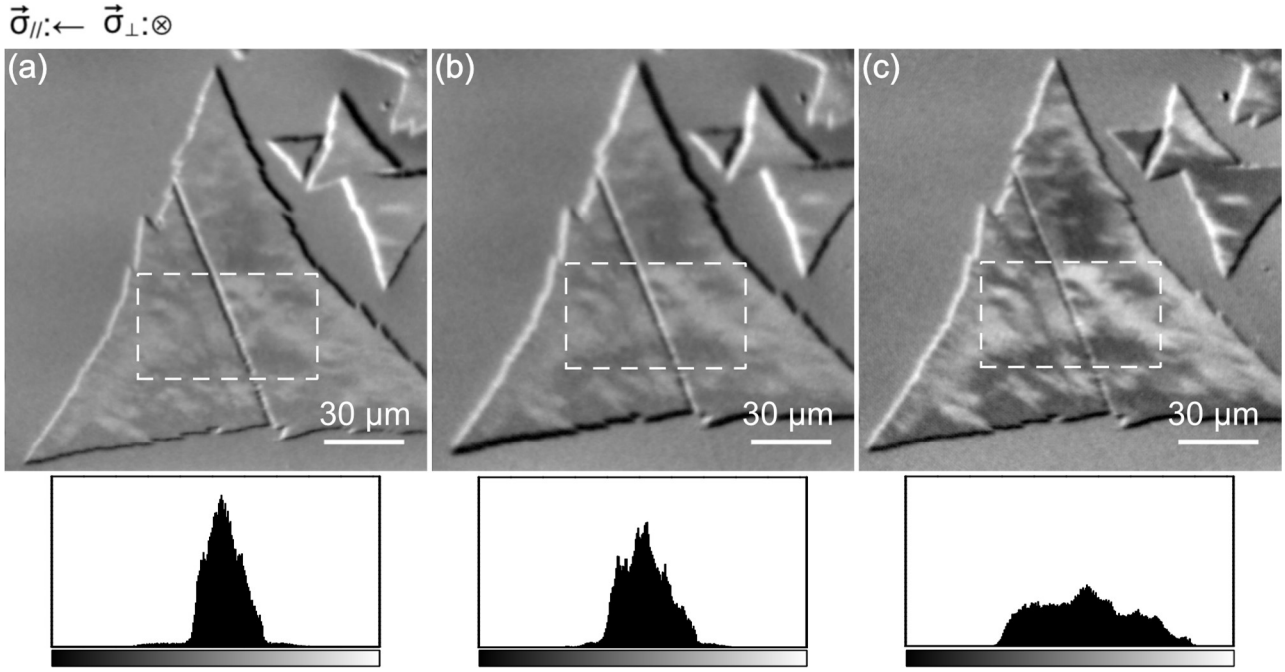

Figure 3: **Co-thickness dependence**. XMCD images of Co with thicknesses of (a) 5 ML, (b) 7 ML, and (c) 9 ML. The histograms below each image measure the grayscale distribution in the region enclosed by the dashed squares in each of the histogram corresponding XMCD images. The domains in (a), (b), and (c) tend to be identical but the color contrast becomes larger. Note that the grayscale is limited to the range of 0 to 255 and the three chosen squares have the same area. The presence of several peaks in the histogram implies that the magnetization should be in-plane.

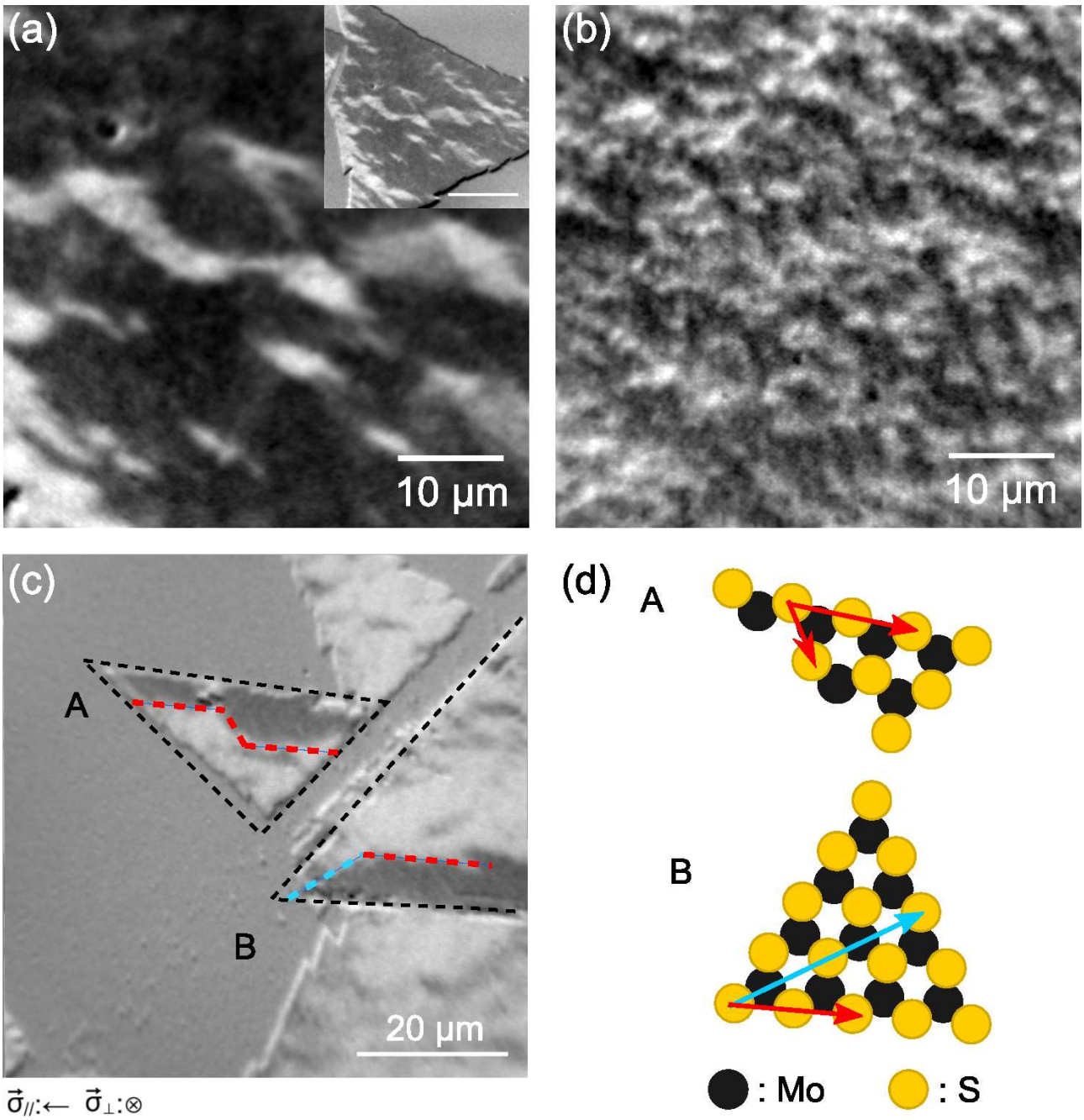

Figure 4: **Magnetic Anisotropy**. XMCD images of (a) a 9 ML Co film on a single grain of monolayer MoS_2 flake and (b) a 9 ML Co film on polycrystalline monolayer MoS_2. The inset in (a) shows its zoomed-out image with a scale-bar set at 30 μm. The domains are larger on the single grain MoS_2 compared to that of polycrystalline MoS_2 (c) The domain boundaries present preferential directions, parallel either to zig-zag (red) or armchair direction (blue) as clearly seen in the corresponding MoS_2 ball models, A and B, drawn in (d).

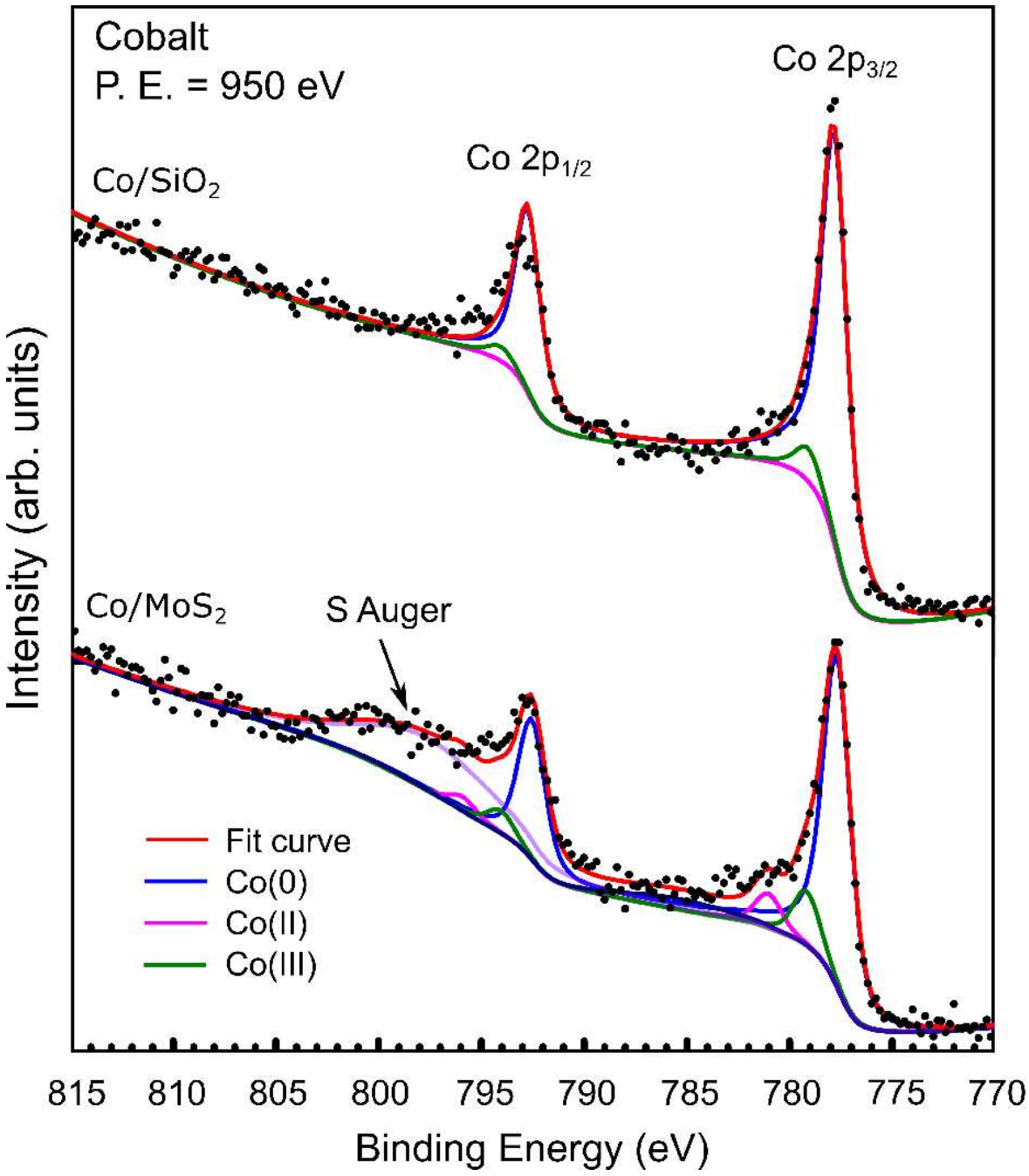

Figure 5: **μ-XPS.** Charge Transfer in Co. The Co 2p μ-XPS spectra acquired on: Co/SiO_2 (upper) and Co/MoS_2 (lower).

REFERENCES

1. Bromley, R. A., Murray, R. B. & Yoffe, A. D. The band structure of some transition metal dichalcogenides: III. Group VI A: trigonal prism materials. *J. Phys. C: Solid State Phys.* **5**, 759-778 (1972).

2. Mattheiss, L. F. Band structure of transition-metal-dichalcogenide layer compounds. *Phys. Rev. B* **8**, 3719-3740 (1973).

3. Coehoorn, R.*, et al.* Electronic structure of $MoSe_2$, MoS_2, and WSe_2. I. Band-structure calculations and photoelectron spectroscopy. *Phys. Rev. B* **35**, 6195-6202 (1987).

4. Geim, A. K. & Grigorieva, I. V. Van der Waals heterostructures. *Nature* **499**, 419-425 (2013).

5. Mak, K. F.*, et al.* Atomically thin MoS_2: a new direct-gap semiconductor. *Phys. Rev. Lett.* **105**, 136805 (2010).

6. Lee, Y.-H.*, et al.* Synthesis of large-area MoS_2 atomic layers with chemical vapor deposition. *Adv. Mater.* **24**, 2320-2325 (2012).

7. Cappelluti, E.*, et al.* Tight-binding model and direct-gap/indirect-gap transition in single-layer and multilayer MoS_2. *Phys. Rev. B* **88**, 075409 (2013).

8. Jin, W.*, et al.* Direct measurement of the thickness-dependent electronic band structure of MoS_2 using angle-resolved photoemission spectroscopy. *Phys. Rev. Lett.* **111**, 106801 (2013).

9. Wang, Q. H.*, et al.* Electronics and optoelectronics of two-dimensional transition metal dichalcogenides. *Nat. Nanotechnol.* **7**, 699-712 (2012).

10. Cheng, R.*, et al.* Electroluminescence and photocurrent generation from atomically sharp WSe_2/MoS_2 heterojunction p-n diodes. *Nano Lett.* **14**, 5590-5597 (2014).

11. Furchi, M. M.*, et al.* Device physics of van der Waals heterojunction solar cells. *npj 2D Mater. Appl.* **2**, 3 (2018).

12. Lan, Y. W.*, et al.* Atomic-monolayer MoS_2 band-to-band tunneling field-effect transistor. *Small* **12**, 5676-5683 (2016).

13. Xiao, D.*, et al.* Coupled spin and valley physics in monolayers of MoS2 and other group-VI dichalcogenides. *Phys. Rev. Lett.* **108**, 196802 (2012).

14. Xu, X., Yao, W., Xiao, D. & Heinz, T. F. Spin and pseudospins in layered transition metal dichalcogenides. *Nat. Phys.* **10**, 343-350 (2014).

15. Roldán, R.*, et al.* Momentum dependence of spin–orbit interaction effects in single-layer and multi-layer transition metal dichalcogenides. *2D Mater.* **1**, 034003 (2014).

16. Mak, K. F., He, K., Shan, J. & Heinz, T. F. Control of valley polarization in monolayer MoS_2 by optical helicity. *Nat. Nanotechnol.* **7**, 494-498 (2012).

17. Cao, T.*, et al.* Valley-selective circular dichroism of monolayer molybdenum disulphide. *Nat. Commun.* **3**, 887 (2012).

18. Wu, S.*, et al.* Electrical tuning of valley magnetic moment through symmetry control in bilayer MoS_2. *Nat. Phys.* **9**, 149-153 (2013).

19. Zeng, H.*, et al.* Valley polarization in MoS_2 monolayers by optical pumping. *Nat. Nanotechnol.* **7**, 490-493 (2012).

20. Zhu, Z. Y., Cheng, Y. C. & Schwingenschlögl, U. Giant spin-orbit-induced spin splitting in two-dimensional transition-metal dichalcogenide semiconductors. *Phys. Rev. B* **84**, 153402 (2011).

21. Ochoa, H. & Roldán, R. Spin-orbit-mediated spin relaxation in monolayer MoS_2. *Phys. Rev. B* **87**, 245421 (2013).

22. Wang, W.*, et al.* Spin-valve effect in NiFe/MoS_2/NiFe junctions. *Nano Lett.* **15**, 5261-5267 (2015).

23. Dolui, K., Narayan, A., Rungger, I. & Sanvito, S. Efficient spin injection and giant magnetoresistance in Fe/MoS_2/Fe junctions. *Phys. Rev. B* **90**, 041401 (2014).

24. Hsu, H.-C.*, et al.* Surface morphology, magnetism and chemical state of Fe coverage on MoS_2 substrate. *Appl. Surf. Sci.* **357**, 551-557 (2015).

25. Hsu, C.-C.*, et al.* Magnetic decoupling of Fe coverage across atomic step of MoS_2 flakes on SiO_2 surface. *J. Phys. D: Appl. Phys.* **50**, 415001 (2017).

26. Garandel, T.*, et al.* Electronic structure of the Co(0001)/MoS_2 interface and its possible use for electrical spin injection in a single MoS_2 layer. *Phys. Rev. B* **95**, 075402 (2017).

27. Wei, D.-H., Chan, Y.-L. & Hsu, Y.-J. Exploring the magnetic and organic microstructures with photoemission electron microscope. *J. Electron Spectrosc. Relat. Phenom.* **185**, 429-435 (2012).

28. Schneider, C. M.*, et al.* Expanding the view into complex material systems: From micro-ARPES to nanoscale HAXPES. *J. Electron Spectrosc. Relat. Phenom.* **185**, 330-339 (2012).

29. Park, W.*, et al.* Photoelectron spectroscopic imaging and device applications of large-area patternable single-layer MoS_2 synthesized by chemical vapor deposition. *ACS Nano* **8**, 4961-4968 (2014).

30. Chen, C.-T., Sette, F., Ma, Y. & Modesti, S. Soft-x-ray magnetic circular dichroism at the $L_{2,3}$ edges of nickel. *Phys. Rev. B* **42**, 7262-7265 (1990).

31. Erskine, J. L. & Stern, E. A. Calculation of the M_{23} magneto-optical absorption spectrum of ferromagnetic nickel. *Phys. Rev. B* **12**, 5016-5024 (1975).

32. Wang, B.-Y., *et al.* Flipping magnetization induced by noncollinear ferromagnetic-antiferromagnetic exchange coupling. *Phys. Rev. B* **85**, 094412 (2012).

33. Stöhr, J. & Siegmann, H. *Magnetism: From fundamentals to nanoscale dynamics*. Berlin: Springer (2006).

34. Please refer to the supplementary information online for the further detailed discussing.

35. Chen, Q., *et al.* Uniformly wetting deposition of Co atoms on MoS_2 monolayer: a promising two-dimensional robust half-metallic ferromagnet. *ACS Appl. Mater. Interfaces* **6**, 16835-16840 (2014).

36. Lu, C.-I., *et al.* Graphite edge controlled registration of monolayer MoS_2 crystal orientation. *Appl. Phys. Lett.* **106**, 181904 (2015).

37. NIST X-ray Photoelectron Spectroscopy Database, Version 4.1 (National Institute of Standards and Technology, Gaithersburg, 2012); http://srdata.nist.gov/xps/.

38. Chen, Y., Zhao, S. & Liu, Z. Influence of the synergistic effect between Co-N-C and ceria on the catalytic performance for selective oxidation of ethylbenzene. *Phys. Chem. Chem. Phys.* **17**, 14012-14020 (2015).

39. Entani, S., Kiguchi, M., Ikeda, S. & Saiki, K. Magnetic properties of ultrathin cobalt films on SiO_2 substrates. *Thin Solid Films* **493**, 221-225 (2005).

40. Ye, J., *et al.* Synthesis of Co-doped MoS_2/graphene hybrids as enhanced electrocatalysts for the hydrogen evolution reaction. *RSC Adv.* **6**, 104925-104932 (2016).

41. Prinz, G. A. Stabilization of bcc Co via epitaxial growth on GaAs. *Phys. Rev. Lett.* **54**, 1051-1054 (1985).

Supplementary Information is linked to the online version of the paper at www.nature.com/nature.